Aalborg Universitet

AALBORG UNIVERSITY

Standardizing practices and flux predictions in membrane science via simplified equations and membrane characterization

Tiraferri, Alberto; Malaguti, Marco ; Mohamed, Madina; Giagnorio, Mattia; Aschmoneit, Fynn Jerome

ARTICLE   OPEN

Standardizing practices and flux predictions in membrane science via simplified equations and membrane characterization

Alberto Tiraferri [1], Marco Malaguti [1], Madina Mohamed[1], Mattia Giagnorio[2] and Fynn Jerome Aschmoneit [3] ✉

The development of membranes and membrane-based separation processes should be accompanied by a standardization of the protocols applied for membrane characterization and for data analysis. Here, streamlined equations for the estimation of the water flux and of the observed salt permeability coefficient in pressure-driven processes deploying dense membranes are presented. Also, a protocol for the experimental characterization of the transport properties of dense membranes is presented and the results are validated against the proposed equations. The proposed water flux equation is algebraic, whereas the ordinary equation needs to be solved iteratively. Moreover, in contrast to the traditional expression for the solute transport coefficient, which requires estimation of the concentration polarization, the respective equation proposed in this study only requires bulk parameters. Dimensionless variables for water flux, driving pressure, and mass transfer are introduced, and a filtration efficiency is defined, a useful parameter in terms of process design.

INTRODUCTION

The design and the development of the next-generation membranes for reverse osmosis (RO), nanofiltration (NF), forward osmosis, and other separation processes based on high selectivity between water and solutes or among solutes, cannot do without robust membrane characterization protocols and transport modeling tools[1–4]. In turn, the deployment of current and future membranes in high-value applications requires the ability to predict system performance, chiefly membrane flux, in the presence of transport-limiting phenomena, such as concentration polarization[5–7]. While significant efforts are made to synthesize membranes with materials previously unimaginable, these research endeavors are often accompanied by unclear and highly differentiated characterization approaches, which limit the fair comparison between membranes, impair their adoption, and not so rarely thwart the community's confidence in their applicability. In the ideal situation, a standardized, straightforward and robust evaluation procedure including both an experimental protocol and a data modeling strategy would be applied and would allow the evaluation of clear, univocal results by all parties, from materials scientists to the final stakeholders.

In processes utilizing an applied pressure on the feed side of asymmetric, e.g., thin-film composite, membranes (i.e., RO, NF), when the objective of the research is the characterization of a membrane, the approach should provide values for the transport coefficients of the main species, namely, that related to water (also known as water permeance), A, and those related to each solute of interest, B (here referred to as observed salt permeance or as observed salt permeability coefficient), measured under relevant conditions[8–10]. According to the solution-diffusion transport model, these parameters are solely related to the membrane properties and to the interaction between the membrane and the relative species in the feed solution, and they do not depend on

the experimental conditions[11]. More recent models, such as the solution-friction model, have improved our understanding of membrane transport and describe instead a dependence of the observed salt permeability coefficient on feed salt concentration and applied pressure, through the elimination of the assumption of a constant hydraulic pressure across the membrane and by accounting for interactions among water, salt ions, and the membrane[12–14]. Therefore, according to the solution-diffusion model, a uniform B value would be used to compare different membranes. On the other hand, according to the more accurate solution-friction model, attention should be paid that observed salt permeability values are compared only when obtained under the same pressure and salt concentration conditions. Regardless, B remains a powerful and simple parameter to compare different membranes deployed under similar conditions and/or applications. Unfortunately, reports on membrane characterization usually include permeate fluxes and observed rejection rates which, while interesting for practical purposes, are not as comparable and significant as permeance values[15,16]. Also, the related tests are rarely performed under reliably representative conditions for real applications, such as pressure values, hydrodynamics conditions, recovery rates, and feed composition.

On the other hand, when the transport characteristics of a membrane are known, adequate predictions of the water flux become possible under a variety of engineering conditions or applications, also with the goal to support the design of such systems[4,17]. One of the main obstacles for the correct predictions of water flux or for the calculation of the transport parameters, is that concentration polarization must be taken into account[18]. Accounting for concentration polarization means knowing or being able to predict the exact value for the osmotic pressure at the feed membrane surface, π_m, whether in laboratory setups or in full-scale modules[19,20]. The fluid dynamics in the feed channel are

[1]Department of Environment, Land and Infrastructure Engineering, Politecnico di Torino, Corso Duca degli Abruzzi 24, 10129 Turin, Italy. [2]Department of Environmental and Resource Engineering, Technical University of Denmark, Miljøvej 113, Kgs. Lyngby 2800, Denmark. [3]Department of Mathematical Sciences, Aalborg University, A.C. Meyers Vænge 15, 2450 Copenhagen, Denmark. ✉email: fynnja@math.aau.dk

governed by the convection-diffusion equation and the separation characteristics of the membrane. In particular, the solute transport in the membrane-feed channel can be quantified locally or broadly, by means of the mass transfer coefficient k_d. If the mass transfer coefficient is known, the concentration at the feed-membrane interface c_m can be estimated by solving the convection-diffusion equation in the membrane boundary layer, yielding $c_m = c_f \exp(j_w/k_d)$. The usually unknown value of c_m is therefore expressed through the more accessible bulk feed concentration c_f, the water flux j_w, and the mass transfer coefficient. Under the assumptions of ideal thermodynamics, i.e., the osmotic pressure is linearly related to concentration, and of the intrinsic membrane A value being independent of salt concentration and other operating conditions, the osmotic pressures in the bulk feed and permeate, π_f, π_p, and the hydraulic feed pressure p_f define the well-known ordinary water flux equation[21]:

$$j_w = A\left[p_f + \pi_p - \pi_f \exp\left(\frac{j_w}{k_d}\right)\right] \tag{1}$$

This model accurately predicts the water flux under the influence of concentration polarization, when the mass transfer coefficient is known. However, it has one key disadvantage: it is a so-called transcendental equation because the term j_w cannot be isolated. As such, it has to be solved iteratively or numerically, and this necessity somewhat complicates the prediction of water flux under different conditions when salt is present in the feed solution. Such intricacy and reliance on manual calculations often invite errors, dubious approximations, inconsistencies, and significant wasted time.

An important initiative has recently started to make membrane performance data and membrane evaluation results more easily findable, accessible, inter-operable, and reusable (FAIR). One such attempt is the Open Membrane Database (OMD), a web-based interface that collects data about membranes worldwide and "allow the easy exploration and comparison of membrane performance, physicochemical properties, and synthesis conditions"[22]. The OMD website also includes effective explanations and calculations tools for concentration polarization and membrane performance evaluation. Another parallel project is related to the development of the so-called "membrane-toolkit" (https://rkingsbury.github.io/membrane-toolkit/), a software serving as a library of validated calculators, with thorough documentation and high test coverage with the following goals: (i) automate routine tasks around membrane investigation to save time and reduce human error, (ii) promote standardization of membrane characterization, (iii) facilitate the creation and curation of large membrane data sets.

This work fits within these ongoing efforts and its main aims are: to (a) propose and assess a robust experimental protocol and a simplified equation to estimate B from experimental data only based on bulk parameters, as well as (b) to propose and assess a simplified non-transcendental, algebraic, equation used to reliably estimate water fluxes in the presence of concentration polarization. The main hypothesis is that the ordinary water flux equation (1) can be expressed in algebraic form without the loss of significant information following rational approximation. The validity of the simplified algebraic water flux equation is thus evaluated under an ample range of working conditions and tested against the results of the experimental characterization of several membranes following the proposed protocol.

METHODS

The algebraic water flux framework consists of three fundamental elements:

(i) Dimensionless process variables for the characterization of membrane processes allow for better comparability of processes and a phenomenological perspective on membrane processes.
(ii) The central piece of the framework is the algebraic water flux equation providing a simple method for evaluating the filtration efficiency from dimensionless bulk variables.
(iii) Related characterization equations for process characterization and design optimization, using dimensionless bulk variables.

Dimensionless variables for filtration efficiency, pressure modulus, and transportiveness

Dimensionless variables allow for better comparability of membrane processes, as will be shown later. The filtration efficiency J is defined as the ratio of the water flux and the ideal, maximum, water flux that would be obtained without concentration polarization. Depending on the magnitude of the concentration polarization, the filtration efficiency assumes a value between 0% and 100% and therefore represents a quantity for assessing the efficiency of the filtration process. The pressure modulus, P, is defined as the ratio of the net driving pressure and the feed osmotic pressure minus the observed rejection rate, and it is positive for pressure-driven processes. Finally, the transportiveness K is a measure for effectiveness of mixing in the feed channel. It is defined as the mass transfer coefficient, divided by the theoretical counter flow. A large transportiveness indicates good solute mixing. Only in the case of very saline solutes and at slow cross-flow rates, may the transportiveness be smaller than unity. The dimensionless flow variables are:

$$J = \frac{j_w}{A(p_f - R\pi_f)}, \quad P = \frac{p_f}{\pi_f} - R, \quad K = \frac{k_d}{A\pi_f}, \tag{2}$$

where $R = 1 - c_p/c_f$ is the observed rejection. Note that these three variables and the equations proposed in this study are applicable to all membrane configurations, e.g., cross-flow or dead-end systems. This is true also for K, as long as the mass transfer coefficient in the feed channel is known. Note that in the case of unsteady flow, e.g. in dead-end systems, the mass transfer coefficient is time-dependent. Also, note that the three dimensionless variables are calculated using macroscopic experimentally-observed parameters, with the only exception of A. One of the main assumptions of this study is that A is independent of operating conditions, and its definition strictly follows the solution-diffusion model. However, as explained by previous studies discussing the solution-friction model, the friction between water and the membrane, which is independent of salt concentration, dominates the hydraulic pressure drop across the membrane, thus resulting in near-stable water permeability under different operating conditions[12–14]. Therefore, the three variables and the equations proposed in this study are applicable under practical conditions from the point of view of different models used to describe membrane transport.

Equations for process design and membrane characterization: water flux

The dimensionless process variables presented above are used to derive simpler expressions for the water flux and related quantities. The equations presented in this section are based on mathematical derivations, which can be found in the Supplementary Information.

Equation (3) represents the dimensionless version of the ordinary water flux equation (1). This equation is in itself not simpler, nor more expressive than the full water flux equation, since it remains a transcendental function of the filtration efficiency, J. However, it states that the efficiency is one minus

the very right-hand term, which can therefore be directly linked to the effect of concentration polarization. In the limit of perfect solute mixing, $K \to \infty$, the concentration polarization term becomes zero and the filtration efficiency equation reduces to $J = 1$. That relates to $j_w = A(p_f + \pi_p - \pi_f)$, i.e., a perfect filtration efficiency with no concentration polarization[11].

$$J = 1 - \underbrace{\frac{1}{P}\left[\exp\left(\frac{JP}{K}\right) - 1\right]}_{\text{concentration polarization}} \qquad (3)$$

The fundamental problem with this equation is its transcendental character, where the filtration efficiency J is both on the left-hand side and inside the exponential function on the right-hand side. It is shown in the Supplementary Information (Note 1) how the filtration efficiency J can be written as a function of the pressure modulus P and the transportiveness K, where the J stands isolated on the left-hand side:

$$J = 1 - \underbrace{\frac{1}{1 + K} - \frac{PK}{2(1 + K)^3}}_{\text{concentration polarization}} \qquad (4)$$

In contrast to the ordinary water flux equation, this equation is algebraic, and can be conveniently solved without the need for iterative solvers. It is therefore referred to as the algebraic water flux equation, constituting one of the central items of this article. It must be emphasized that the algebraic water flux equation is an approximation to the ordinary water flux equation. It is therefore also based on the classical convection-diffusion model. Similarly to the ordinary equation, it is seen that the concentration polarization term disappears, under the assumption of perfect mixing, $K \to \infty$. On the other hand, when the cross-flow is stagnating, $K \to 0$, the water flux will converge to zero as a consequence of overwhelming external concentration polarization (ECP). In this form, the algebraic water flux equation expresses the filtration efficiency as 'one minus the effect of concentration polarization', that makes it especially convenient for the analysis of membrane processes.

For example, suppose that a lab experiment or that a system is designed with $(P, K) = (4, 6)$, yielding a filtration efficiency of $J \approx 82\%$. That directly implies that 18% efficiency is lost to concentration polarization. These values for P and K could exemplarily relate to a brackish water process with $A = 4$ LMH/bar, $R = 98\%$, $p_f = 12$ bar $\pi_f = 4$ bar, $k_d = 96$ LMH, or a

wastewater process with $A = 10$ LMH/bar, $R = 95\%$, $p_f = 2.3$ bar, $\pi_f = 0.75$ bar, $k_d = 45$ LMH.

For completeness, the water flux is also presented in absolute terms in equation (5). It follows from substituting the dimensionless variables in equation (4). This equation is the algebraic approximation to equation (1).

$$j_w = A(p_f - R\pi_f)\underbrace{\left(1 - \frac{A\pi_f}{A\pi_f + k_d} - \frac{A^2(p_f - \pi_f R)\pi_f k_d}{2(A\pi_f + k_d)^3}\right)}_{=J} \qquad (5)$$

Comparing equations (4) and (5) demonstrates the benefit of using dimensionless variables as they not only exemplify physical meaning, but also improve readability and conciseness. Equation (5) shall remain here as a stand-alone result, while the remaining of this article is concerned with the dimensionless water flux equation (4). As the algebraic water flux equation (4) is an approximation, it must be analyzed how much it deviates from the ordinary water flux equation.

Error quantification. Figure 1a presents contour maps of the filtration efficiency and Fig. 1b shows the deviations introduced through the approximations in the algebraic water flux equation. Both contour plots deploy the same, representative ranges of pressure modulus P and transportiveness K. The dashed and solid lines in Fig. 1a show the filtration efficiency for the ordinary water flux equation (3) and the algebraic water flux equation (4), respectively. Qualitatively, it is seen that both equations predict that the filtration efficiency increases significantly for increasing K values and moderately for increasing P values. Furthermore, it is seen that the approximated, algebraic water flux equation deviates from the ordinary equation for increasing P values. For filtration efficiencies $J > 60\%$, the algebraic equation underestimates the water flux, while it overestimates the water flux where $J < 60\%$. Figure 1b illustrates a quantification of how severe the model deviations are. The continuous contour lines indicate the relative error of calculating J with equation (4) (algebraic) vs. calculating J with equation (3) (ordinary). The derivation of the algebraic water flux equation makes two central assumptions; see Supplementary Information. The contour lines of relative error illustrate nicely how these underlying assumptions create two regions of inaccuracies: The region $(P > 5, K > 3)$ relates to assumption 1, and the region $(K < 3)$ relates to assumption 2, see Supplementary Information. While inaccuracies in the top-
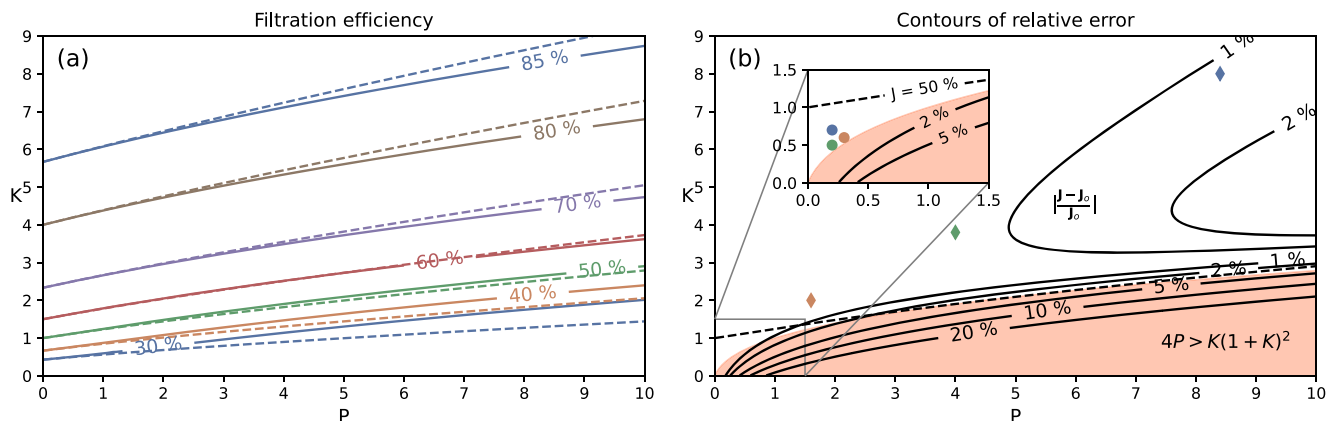
Fig. 1 The filtration efficiency according to ordinary and algebraic equations and the magnitude of inaccuracy of the algebraic water flux equation. a The solid lines follow the algebraic water flux equation (4). The dashed lines follow the ordinary water flux equation (3). The algebraic water flux equation under-predicts the water flux above $J = 60\%$ (conservative estimate). Below $J = 60\%$ it overestimates the ordinary water flux. **b** The black contour lines indicate where the algebraic water flux equation introduces approximation errors: Relative difference (%) between the results of water flux, J_0, obtained from ordinary water flux equation (3) and the values of water flux, J, obtained with algebraic water flux equation (4). The region of significant inaccuracies coincides reasonably well described with the area $4P > K(K+1)^2$. The dashed line indicates the efficiency contour of $J = 50\%$. The disc and diamond shapes relate to the exemplary processes in Table 1.

Table 1. Exemplary membrane processes and validity of the algebraic water flux equation.

	Wastewater		Brackish water		Seawater	
A (L m^{-2}h^{-1}bar^{-1})	10		4		1.1	
Observed rejection	0.900		0. 980		0.997	
Recovery rate	0.85		0.75		0.50	
Channel position	Inlet (feed)	Outlet (retentate)	Inlet (feed)	Outlet (retentate)	Inlet (feed)	Outlet (retentate)
p_f (bar)	7	6	20	19	70	69
π_f (bar)	0.75	5	4	16	27	54
Average π_p (bar)	0.075	0.5	0.08	0.32	0.08	0.16
k_d (L m^{-2} h^{-1})	60	30	60	30	60	30
P	8.43	0.30	4.02	0.21	1.60	0.28
K	8.00	0.60	3.75	0.47	2.02	0.51
$4 \cdot P < K \cdot (1+K)^2$?	y	y	y	y	y	y
J	0.84	0.35	0.72	0.30	0.61	0.31
Symbol	◆	●	◆	●	◆	●

Operating conditions and feed inlet/outlet flow variables for three membrane processes. The operation conditions were chosen conservatively, in order to estimate the validity of the algebraic water flux equation in extreme industrial applications. The respective (P, K) operation points are indicated in Fig. 1b, using the symbols defined in the last table row.

right region are negligibly small, the region for diminishing K values indicates close error contours and hence, significant inaccuracies of the algebraic water flux equation. The region of great inaccuracies can conveniently be related to the empirically found relation $4P > K(1+K)^2$, which corresponds to the red area in Fig. 1b. The black dashed line indicates the contour of $J = 50\%$ efficiency. It is seen that for $P > 3$ the region of increasing inaccuracies corresponds to $J < 50\%$. This allows us to define a practical condition for the validity of the algebraic water flux equation as $4P < K(1+K)^2$, or, as a rule of thumb, $J > 50\%$, where $P > 3$.

Error discussion. In practical terms, the validity condition basically renders the algebraic water flux equation invalid for very small mass transport coefficients in the feed chamber/channel only, where the concentration polarization is extreme. It is shown in the following that this limitation is of little practical significance. Table 1 presents process exemplifications of three typical medium and high-pressure membrane applications, namely, seawater, brackish water, and wastewater desalination. For each of these applications, the table presents typical operating conditions and the flow variables at the feed inlet and outlet of a membrane. The values of the mass transfer coefficients were chosen conservatively (i.e., lower than typical values), causing significant concentration polarization in each of the processes. From the operation conditions follow the (P, K) operation points at the inlet and outlet, using the definitions in equation (2). The third-last row in Table 1 indicates that all (P, K) operation points pass the validity condition, see also Fig. 1b for locations of these operation points in the map of relative errors. The filtration efficiency J will therefore be very well-approximated with the algebraic water flux equation (4). It is seen in the second-last row that the filtration efficiency is much greater at the inlets, while it reduces to only $30-35\%$ at the outlet, which is due to the build-up of concentration polarization caused, in turn, by the high concentration of the retentate stream (and a small mass transfer coefficient in cross-flow systems due to low flow rates in the feed channel at the outlets). In conclusion, only if concentration polarization is impractically high, the algebraic equation is not accurate.

However, such conditions are virtually never found in real or in laboratory applications[23]. The algebraic water flux equation therefore accurately reproduces the prediction of water flux of the ordinary equation for a wide range of realistic K and P. Its accuracy is impaired only for conditions that are rarely found in laboratory or full-scale applications.

Equations for process design and membrane characterization: observed salt permeability coefficient

Focusing attention on the simplification of an expression to calculate the observed solute permeance of the membrane, B. Note that in this study, B is regarded as an experimental-based parameter and does not necessarily refer to an intrinsic membrane property. B is defined as the value of salt permeance observed under specific and fixed operating conditions. It should be reminded that this parameter requires accounting for concentration polarization, since it depends on c_m, the feed concentration at the membrane interface, which is affected by the concentration polarization. This is commonly accomplished through indirect experimental-based estimation of the solute concentration at the feed/membrane interface and/or using the mass transfer coefficient, k_d. The mass transfer coefficient k_d is a complex quantity in the sense that its value depends on the operation conditions through, e.g., the cross-flow velocity, the feed concentration, and the solute's diffusion coefficient, but also on the membrane geometry through, e.g., channel widths, spacers, fouling[24]. However, a reasonable estimate for the mass transfer can be obtained as a function of the other process variables. Therefore, within the framework of the dimensionless process variables, the transportiveness K can be expressed as a function of the filtration efficiency J and the pressure modulus P as:

$$K = \frac{JP}{\underbrace{\ln(1 + P(1-J))}_{CP_{mod}}}$$

(6)

This expression for the transportiveness follows directly from the dimensionless water flux equation (3), see derivation in the Supplementary Information. It is therefore not an approximation

and no errors are introduced. The argument in the logarithm function of equation (6) is identified as the concentration polarization modulus π_m/π_f, which yields this very simple expression for the concentration polarization modulus:

$$CP_{mod} = 1 + P(1 - J) \qquad (7)$$

Note that, quite significantly, in this way CP_{mod} and K are determined without the need to know c_m or π_m, i.e., without the need to know or estimate the mass transfer coefficient k_d. On the contrary, equation (7) can be used to estimate π_m and B in a simple manner and only considering bulk values of the parameters, by applying the following equation:

$$B = j_w \frac{1 - R}{CP_{mod} - 1 + R} \qquad (8)$$

The derivation of the above equation can be found in the Supplementary Information. It does not include any approximations and will therefore not introduce inaccuracies. Importantly, equation (8) deploys J and P, which are based on readily available bulk parameters, only. Additionally, as already mentioned above, this equation allows the calculation of an observed salt permeability coefficient, not necessarily an intrinsic membrane parameter. No assumptions are made in this study regarding the behavior of B as a function of operating conditions. When conditions change, e.g., the salt concentration is higher in the feed solution, the solution-friction model predicts a different, e.g., larger, value for B. In fact, this behavior would produce condition-specific experimentally accessible values of j_w, CP_{mod}, and R, which are applied in equation (8) and translate into a respective condition-specific value of the observed salt permeability coefficient, B. In this sense, this simple equation based on experimentally available bulk parameters is applicable from both the point of view of the solution-diffusion and the solution-friction model. It should be noted that, according to the solution-friction model, the observed salt permeance, here referred to as B, approaches the value of an intrinsic membrane salt permeance when membranes are not charged or when the feed salt concentration is high compared to the membrane charge density.

A robust protocol for the experimental characterization of membrane transport

In this section, a protocol aimed at characterizing the transport properties of a membrane comprising a dense active layer is proposed. Such a protocol should be easily reproducible and practical so as to be used as a standard practice, should be as simple as possible while being as detailed as necessary, and should be reliable and consistent in terms of outcomes and for that reason involve overdetermined data. These characteristics are collectively referred to as 'robust'.

Setup and operating conditions: the membrane characterization rig should include systems to control temperature, pressure, and, when relevant, cross-flow. When the membrane cross-flow cell is small, each of these parameters may be measured at the feed inlet or concentrate outlet, only. However, for large cross-flow membrane housings, both inlet and outlet values should be considered. Experimentalists should use deionized water as a feed solution to determine A and should prepare a stock solution of concentrated salt or salt mixture to be dissolved and diluted into the deionized water solution to determine rejection rates and B. Experimentalists should be able to maintain steady-state when needed, for example by running a cross-flow rig in closed-loop, i.e., concentrate and permeate streams recirculated into the feed tank; however, any configuration that allows keeping conditions (e.g., composition of the feed tank) constant in time is suitable. Probes or analytical instrumentation for pH and solute measurements are necessary to ensure the desired water composition and

to measure rejection rates. The conditions deployed for membrane characterization, including feed pressures as well as the nature and the concentration of the solute(s) in the feed solution, should be chosen in the range that is relevant or representative of the specific application for which a membrane has been fabricated. An important parameter related to water composition is pH, which should be checked and adjusted to the desired value. With regard to the sampling of the feed and permeate solutions, attention shall be paid that the total volume of all samples collected during the test is negligible compared to the initial feed solution volume.

Execution of the test: a first compaction step should be performed, using deionized water as feed solution (phase 0). This step should be run at a higher feed pressure compared to the pressure values subsequently used for characterization, and until a steady-state in flux is achieved. At this point, water flux should be measured at varying pressure, each time at steady-state (phase 1). The authors suggest taking measurements with at least three different feed pressures. Subsequently (phase 2), the concentrated stock solution containing solute(s) should be added into the feed tank and pH adjusted to obtain the desired feed composition. This step should be done while letting the system run. For the characterization phase of membrane selectivity, it is advised to obtain different values of water flux and solute concentrations at various combinations of feed-applied pressure and mass transfer coefficient in the feed channel/chamber (obtained, e.g., varying the cross-flow velocity in cross-flow configurations). The authors suggest using at least three combinations. Based on the current understanding of membrane transport, water flux should always increase with feed pressure at a constant value of the mass transfer coefficient, due to an increase in bulk driving force in the feed channel/chamber, and it should also increase at increasing value of the mass transfer coefficient if the feed pressure remains constant, due to lesser concentration polarization. For analogous reasons and according to currently available transport models, observed rejection should increase if either feed pressure or mass transfer coefficient is increased. These trends may be used to verify whether the experiment is running in accordance with expectations. It is imperative that all values of water flux and solute concentrations used for subsequent analyses are recorded when the system is at steady state. Therefore, a sufficient amount of time should be allowed upon each change of conditions, also to make sure that all tubings/pipings are well flushed with the solutions relative to the new conditions obtained after changing the parameters.

Analysis: The water flux values obtained with deionized water in phase 1 should be fit with a line and this line should pass through the point of zero flux for zero applied pressure (origin of the flux vs. feed pressure graph). If the intercept at zero pressure is significantly distant from the zero value, determination of A may not be accurate and this result may be due to insufficient compaction of the membrane, membrane defects, or experimental deviations occurred during the test. The A value is the slope of the line that best fits the water flux data and that passes through the zero-zero point. For the determination of membrane selectivity from the data collected in phase 2, rejection rates of each solute under each condition are calculated using the concentrations of that solute determined in the feed sample and in the permeate sample, both related to the same time of sampling. Note that when a proxy parameter is used in place of solute concentration, for example, electrical conductivity in place of salinity, experimentalists should consider that the proxy parameter may not correlate linearly with the actual parameter in the entire spectrum of values relevant to the test. Therefore, the direct substitution of one with the other in the equation used to calculate rejection rate may provide inaccurate results. A calibration curve providing the exact correlation between the

Table 2. Experimental conditions for the characterization of the six membranes.

Membrane	Compaction	Phase 1		Phase 2					
	Applied pressure (bar)	Feed Solution	Applied feed pressures (bar)	Feed solution (pH 8.0)	Step 1 p_f (bar) cfv (cm/s)	Step 2 p_f (bar) cfv (cm/s)	Step 3 p_f (bar) cfv (cm/s)	Step 4 p_f (bar) cfv (cm/s)	Step 5 p_f (bar) cfv (cm/s)
SW-1 SW-2 SW-3	65	Deionized water	65, 55, 45, 35	32 g/L NaCl	**55** 57.4	**55** 28.7	**45** 57.4	**45** 28.7	**35** 14.4
BW-1	20		20, 15.5, 10, 5	2 g/L NaCl	**15.5** 57.4	**15.5** 28.7	**10** 57.4	**10** 28.7	**5** 7.7
BW-2	10		10, 8.6, 4.3, 3		**8.6** 57.4	**8.6** 28.7	**4.3** 57.4	**4.3** 28.7	**3** 7.7
NF	6		6, 4.3, 3.4, 2	2 g/L MgSO$_4$	**4.3** 57.4	**4.3** 28.7	**3.4** 57.4	**3.4** 28.7	**2** 7.7

proxy and the actual parameter should be determined in advance and then applied to translate the proxy parameter into the actual concentration. A value of B can be thus obtained for each solute and for each operating condition, by applying equation (8) proposed in this study. It is important to highlight here, once again, that according to the solution-diffusion model, all B values obtained for the same solute in phase 2 are supposed to be equal, regardless of the conditions: thus, according to this model, an average value may be presented. However, more recent and accurate models, e.g., the solution-friction model, suggest that observed B values are not intrinsic to the membrane but they depend also on the operating conditions: thus, presenting an average value is not relevant or correct, and separate observed B values obtained with equation (8) shall be presented, together with the conditions under which they were measured.

Proposed protocol in action: experimental conditions and analyses applied in this study

The transport properties of various polyamide membranes characterized by active layers of different densities were evaluated using a laboratory-scale cross-flow unit[25]. The unit comprises a high-pressure pump, a feed tank, a flat membrane housing cell, and a chiller with heat exchanger coils immersed in the feed tank for temperature control. The effective membrane active area was 20.1 cm^2 and the temperature was constant at $23 \pm 0.5\,°C$. Membranes suitable for processes classifiable as seawater reverse osmosis (SW), brackish water reverse osmosis (BW), and nanofiltration (NF) were deployed. Prior to each experiment, the membrane sample was immersed in water overnight. The filtration tests consisted of two different phases: initially, deionized water (resistivity $> 10^7$ Ohms) was used as feed solution to evaluate the water permeance of the membrane, A; subsequently, an appropriate volume of NaCl stock solution (stock solution concentration = 5 mol/L) or of MgSO$_4$ stock solution (1 mol/L) was directly added into the feed tank to evaluate rejection rates and the solute transport coefficient, B. The pH was fixed at 8.0 by addition of a minimal amount of buffer compound (NaHCO$_3$) and via adjustment with NaOH. The solute concentrations were consistent with those typically utilized by membrane manufacturers for standard membrane testing and commonly reported in the specification sheets.

In the first phase, the applied feed pressure, p_f, was changed to obtain different values of the water flux as a function of p_f with a feed solution of deionized water. In the second phase, both p_f and the cross-flow velocity (cfv) were changed to obtain different measurements of the permeate flux and of the solute rejection in the presence of solutes in the feed solution. Specifically, three cfv values were investigated referred to as high, medium, and low cfv.

These values were chosen because they are consistent with those typically encountered in spiral-wound elements installed in reverse osmosis and nanofiltration plants and consistent with diminishing flow rates along the elements within the plant. The values of p_f and solute concentration were chosen according to the density of the membranes, higher for the membranes with denser active layers and lower for the ones with lower expected rejection. All the testing conditions can be found in Table 2. According to currently available models, the observed rejection, R, is a function of applied feed pressure and feed salt concentration, and is also affected by concentration polarization, which, in turn, is influenced by hydrodynamics conditions, e.g., cross-flow velocity[26].

In the beginning of each test, the membrane sample was compacted with deionized water as feed solution at the highest value of applied pressure until the permeate flux reached a steady-state (generally 2–3 h)[27]. In this first phase involving deionized water as feed solution, p_f was then lowered in a stepwise fashion. In each step, the pressure was changed gradually to avoid shocks in the system and to the membrane, and the water volume passing through the membrane was then measured by means of a computer-interface balance; see also Fig. 2a for an example of experimental data related to membrane "SW-1". The pure water flux was calculated by dividing the volumetric permeate rate, obtained at steady-state (reached typically after only a few minutes), by the membrane active area. A was determined as the slope of the best fitting line for the water flux data as a function of p_f, with the line passing through the origin (Fig. 2b). In the second phase, after addition of solute in the feed solution, five different steps were performed under operating conditions consisting of different combinations of the same values of p_f investigated in the first phase and of three cfv values (Table 2). Solute concentrations in the feed and permeate streams were calculated from conductivity values measured using a conductivity meter (Oakton CON 450), calibrated for each salt. The permeate flux, j_w, was calculated by dividing the volumetric permeate rate by the membrane area. R, was then computed from the concentrations determined in bulk feed, c_f, and in the permeate stream, c_p, as

$$R = 1 - \frac{c_p}{c_f} \tag{9}$$

The observed rejection rates and the permeate fluxes were always measured at steady-state (reached typically after 10–15 min after each change of condition but probed after ~20–25 min from each change of conditions). Therefore, within each step, i.e., for each combination of p_f and cfv, the values of these parameters were always constant in time, within experimental error. Two separate measurements were performed, distanced 10–20 min from each other, and the values were averaged. Except for collection periods,
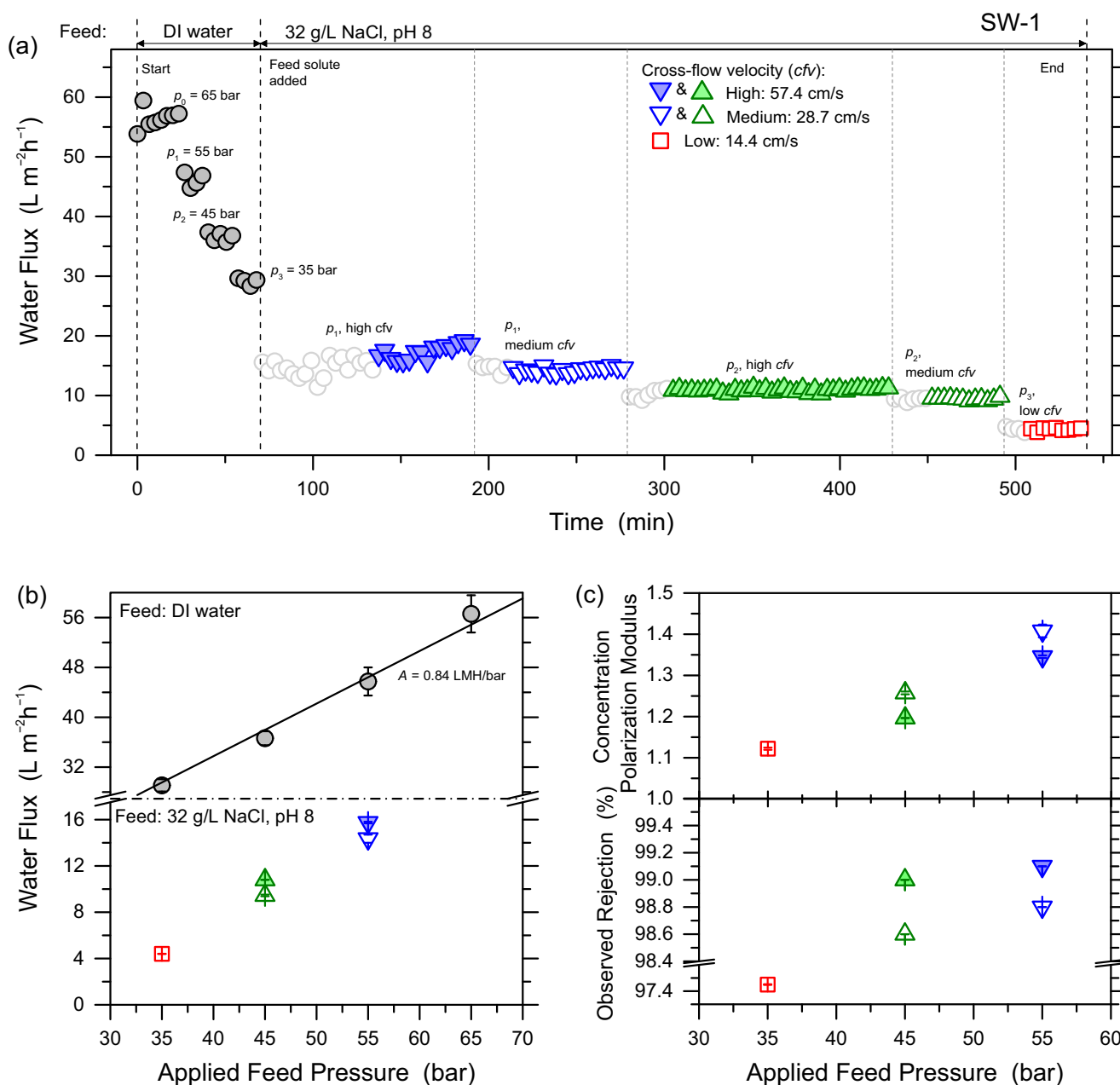
Fig. 2 Results of characterization experiment performed with representative seawater reverse osmosis membrane, SW-1, at near 0% recovery rate. a Water flux as a function of time, showing the various phases and steps. Phase 1 with deionized water as feed solution; phase 2 with 32 g/L NaCl as feed solution (pH 8.0). The fitting line goes through the origin, i.e., no flux at no applied pressure. Empty circles in phase 2 refer to stabilization periods upon changes in feed pressure or cross-flow velocity. **b** Average of flux data measured in the various phases and steps at steady-state, as a function of applied feed pressure; note that the y axis has a break from 18 to 28 $Lm^{-2}h^{-1}$ (LMH). **c** Average of (bottom) observed rejection (%) and (top) concentration polarization modulus, computed for the various steps in phase 2, as a function of applied feed pressure. Note that the y axis of the inset related to the observed rejection has a break from 97.6 to 98.4%. In all graphs, gray circles refer to deionized water as feed solution, downward blue triangles to steps with saline feed solution and feed pressure of 55 bar, upward green triangles to steps with saline feed solution and feed pressure of 45 bar, red squares to a step with feed pressure of 35 bar and low cross-flow velocity. For the two higher pressure values, colored symbols refer to high cross-flow velocity while empty symbols to medium cross-flow velocity. Values plotted in **b** are averages of individual flux values observed during at least 20 mins of operation, all under steady-state conditions. Values plotted in **c** are averages of three individual rejection values, and the averages of the respective values of the concentration polarization modulus, obtained for each step under steady-state conditions. Error bars represent one standard deviation of each of those data samples. The temperature was kept constant at 23 ± 0.5 °C.

both the concentrate and the permeate streams were recirculated back into the feed tank. In the end, B was computed from experimentally available bulk data: first, J and P were calculated from the input or measured data of the experiment. Then, equation (7) was applied to calculate the concentration polarization modulus. Finally, B was obtained using equation (8).

RESULTS AND DISCUSSION
Results of experimental membrane characterizations
Figure 2 presents the experimental results obtained with SW-1, as representative membrane. Figure 2a shows the water flux data measured as a function of time in the various phases and
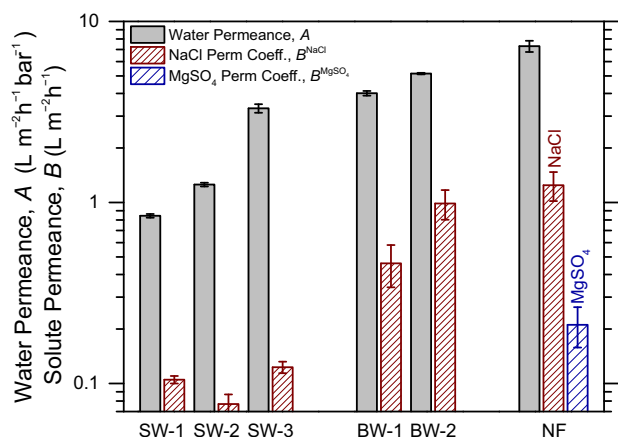
Fig. 3 Observed transport parameters, *A* and *B*, computed from experimental values for the six membranes, from the least permeable to the most permeable from left to right. Gray solid bars refer to *A*, while patterned bars to *B*. All membranes were tested in the presence of NaCl in the feed solution, except the NF membrane, which was also tested in the presence of $MgSO_4$ in the feed solution. Note that the *y* axis is in logarithmic scale. Each water permeance value is the slope of the line fitting the average water fluxes observed as a function of applied feed pressure for a given membrane, while the error bar represents the confidence interval. Each solute permeability coefficient is the average of values obtained in the various steps characterized by different combinations of pressure and cross-flow velocity for a given membrane, with error bars representing one standard deviation of those values.

steps of the experiment. The average water flux data obtained at steady-state in the initial phase of the test is thus reported in Fig. 2b as a function of p_f, where the best fitting line passing through the origin is shown for the calculation of *A*. Figure 2c presents the values of CP_{mod} and *R* (NaCl) evaluated in the five steps of the second testing phase as a function of p_f, in the presence of 32 g/L NaCl in the feed solution (pH 8.0). As expected from theoretical considerations, the permeate flux increased with increasing feed pressure. Consequently, the observed NaCl rejection and the CP modulus also increased. More interestingly, flux and rejection data increased slightly but significantly with increasing cfv at a given value of p_f, thus the value of CP_{mod} decreased. Higher cfv increased the mixing in the feed channel, reducing the thickness of the unmixed boundary layer and reducing the magnitude of ECP[28]. This phenomenon translated into a lower solute concentration at the feed-membrane interface, c_m, which in turns allows a higher effective driving force and lower salt passage across the membrane active layer. These observations were consistently achieved for all membranes, suggesting the reliability of the experimental protocol and the accordance between experimental results and conceptual understanding of the phenomena underlying mass transport across the active layer of asymmetric membranes[21].

Figure 3 summarizes the results in terms of *A* and average *B* for all membrane types. The data are plotted for the six membranes, from the least permeable to the most permeable one from left to right. Just for simplicity and conciseness, the observed salt permeances are here presented as average values for each of the membrane. The individual values of *B*, obtained under each operating condition, can be found in the Supplementary Information. As expected, the highest productivity is achievable with NF membranes, followed by BW and SW membranes, respectively. The values of average *B* correlate well with those of parameter *A*, except for SW-2, which displayed both better productivity and rejection rate than SW-1. Note that

the value of average *B* estimated for NaCl with the NF membrane is significantly higher than that estimated for $MgSO_4$, since the latter solute includes a divalent cation, hence associated with better rejection[29]. More importantly, note that the standard deviations for parameter *B* are relatively small, i.e., low coefficient of variation, despite the fact that these are the average of the five different steps conducted at varying feed pressure and cfv combinations.

Analysis of the filtration efficiency using the algebraic water flux equation

Figure 4 shows the experimental data in the framework of the dimensionless variables, while the unprocessed experimental data are found in the Supplementary Information (see Tables). The curves are contours of the pressure modulus in a $J−K$ map, calculated with the algebraic water flux equation. Apart from the SW-3 data, all data reside in regions where the accuracy of the algebraic water flux equation is at least 99% (97% for the BW-1 membrane). Hence, the figure indicates how well the experimental data adhere to the convection-diffusion model of polarization, as well as how robust the data are in terms of experimental estimation of the hydrodynamics parameters.

A first take-home message from the graphs is that the experimental data are much more in line with the currently available transport models as the density of the membrane active layer increases. Note that the scale of the y-axis is different for the various graphs, with SW-1, SW-2, SW-3 utilizing a smaller range of *J*. This result is consistent with theoretical expectations, since mechanisms of partition of the solvent and of the solutes in the membrane and their diffusion across the active layer become relatively less important compared to other mechanisms of transport, e.g., Donnan exclusion, as the ratio between species and membrane pores is reduced[30]. Even more importantly, in this work, the model was computed assuming that the reflection coefficient is equal to 1, i.e., impermeable solute, which is only a fair approximation for high-rejection membranes[31]. Note that the experimental data almost always sit above the theoretical curves for all membranes, i.e., higher *J* values, and that for the NF membrane the consistency of the data with the theoretical curves improves for $MgSO_4$ compared to NaCl. Both these observations indicate that higher rejection rates undoubtedly allow for safely neglecting the reflection coefficient. When considering the effect of *K*, namely, of hydrodynamics, note that the width of the horizontal error bars imply some level of uncertainty in accurately estimating the value of the mass transport coefficient, one of the main obstacles of membrane characterization, also highlighted above.

Additional noteworthy conclusions can be drawn by assessing the absolute values of *J*, which may be thought of as filtration efficiency or, in other words, how much of the nominal driving force actually goes into producing a water flux. It is important here to underline the difference between filtration efficiency, which refers to the inner workings of a membrane-based system, and absolute productivity, which refers to the amount of product water obtained per unit of time from the same system. While the two variables are connected, the latter is what water utilities are most concerned with and it represents a design objective of the plants, while the former is associated with the means to achieving these objectives. Looking at the behavior of three seawater membranes (SW-1, SW-2, SW-3), all tested at the same value applied feed pressures, the filtration efficiency dropped dramatically from the least permeable to the most permeable membrane, despite the fact that the water fluxes were obviously higher with the latter. This observation implies that attempting to increase flux above a certain range by applying a high applied feed pressure, produces only
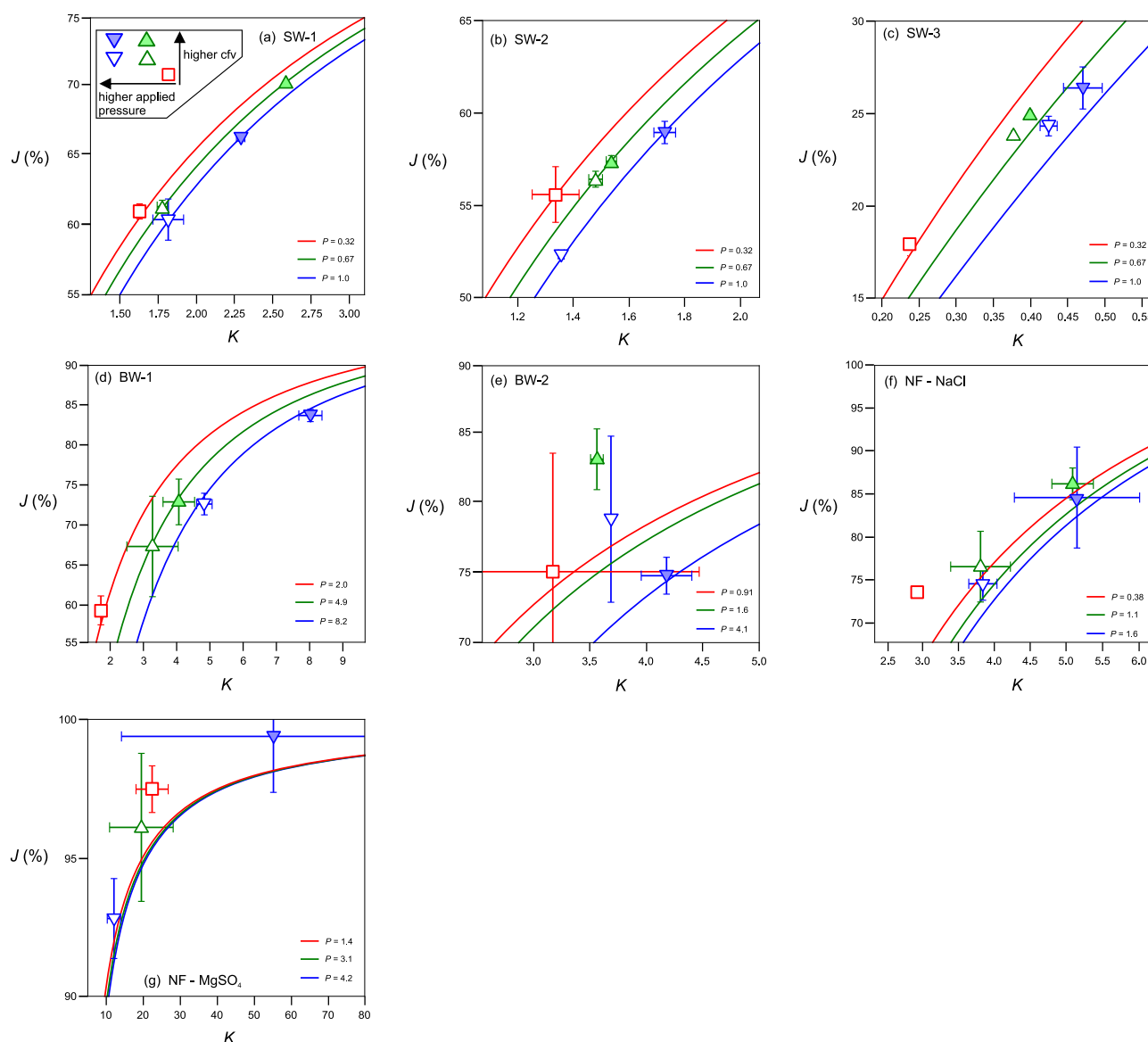
Fig. 4 Experimental results plotted in terms of *K* and *J*, and comparison with the predictions from the algebraic water flux equation. Data are plotted for different membranes in the various graphs, namely, **a** SW-1, **b** SW-2, **c** SW-3, **d** BW-1, **e** BW-2, **f** NF with NaCl in the feed solution, **g** NF with MgSO₄ in the feed solution. Data points are plotted with the same symbols adopted in Fig. 2. The three curves represent the results from the implementation of the algebraic equation (4) for three different values of *P*. Each data point is the average of values obtained in the various steps characterized by different combinations of pressure and cross-flow velocity for a given membrane, with error bars representing one standard deviation of those values. The operation conditions for the respective experiments are indicated in Table 2, in the 'Phase 2' columns.

marginal returns, as the increase in flux brings about a sustained concentration polarization that in turn limits the flux increase itself. Therefore, the energy expense associated with higher feed pressures is not entirely justified, implying that the driving force should be adjusted for each membrane water permeance to be within a certain range, if the goal is to improve efficiency. In real applications, the system productivity is often set by the needs of an industry or a community and the degree of freedom in adjusting filtration efficiency may be lower. However, the results of this study suggest that an increase in membrane area may be more advantageous than that of applied feed pressure, to maintain overall productivity while also increasing efficiency. Indeed, economic considerations are outside the scope of this study, and they must be taken into consideration for real-scale operation.

Application of the algebraic equation in process design and membrane characterization

Figure 5 presents sensitivity maps from the implementation of equations presented above in terms of various interdependencies among *K*, *P*, *J*, and *CP*ₘₒd. Note that such maps do not attempt to aid in overall system-scale design, which should be performed using appropriate modeling tools and should account for the flux and concentration profiles along the entire plant (also considering different stages, passes, recirculations, and bypasses). However, the maps may be used to estimate individual water flux values related to specific combinations of operating conditions (hence, if desired, every water flux value in its changing profile along a membrane plant). Also, the maps nicely illustrate the underlying principles and implications of the algebraic equation and the usefulness, and indeed limitations, of the dimensionless parameters introduced in this study.
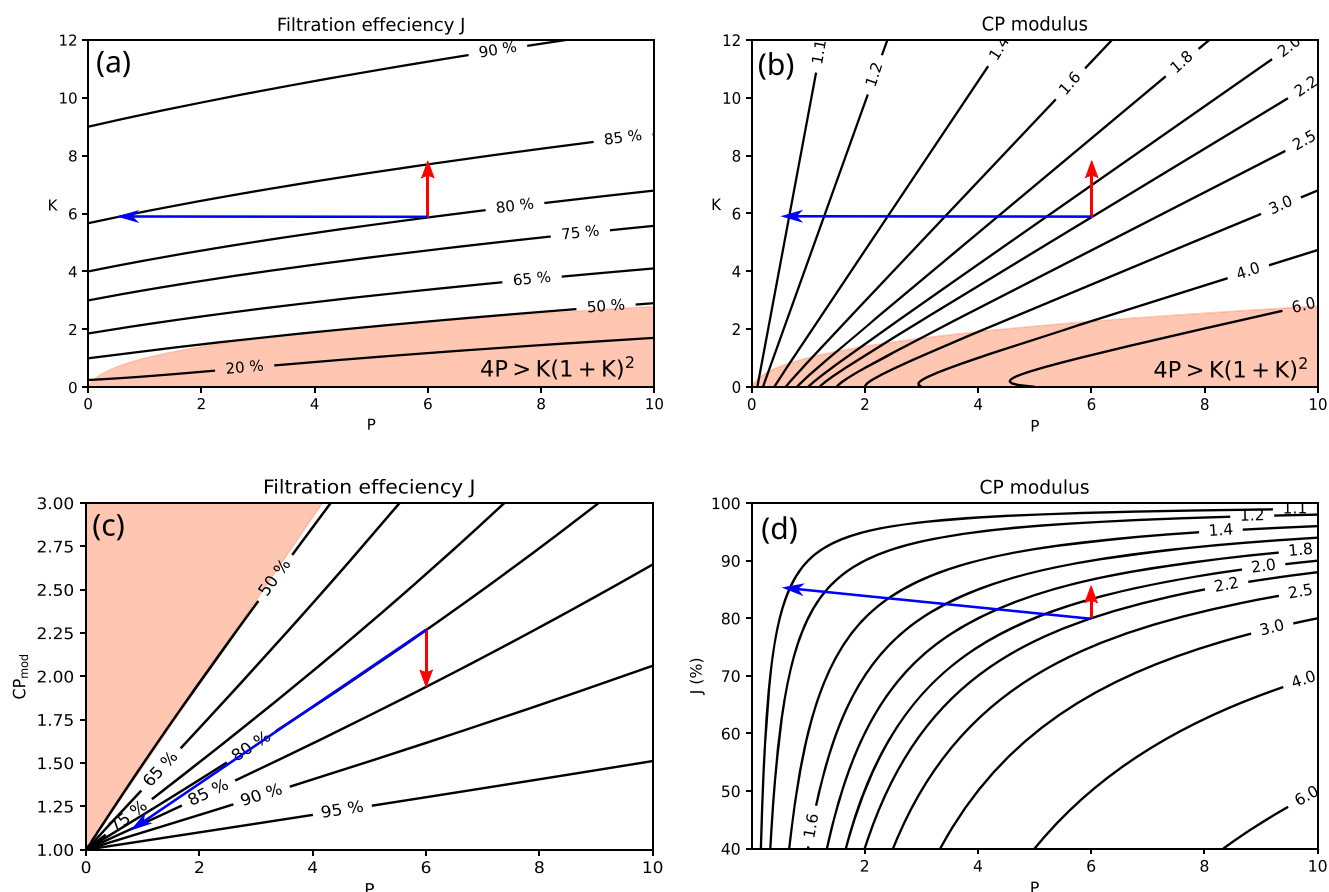
Fig. 5 Sensitivity analyses of filtration efficiency and concentration modulus. a, c contour plots of filtration efficiency J as a function of the pressure modulus P and the transportiveness K (**a**) or the concentration modulus CP_{mod} (**c**). **b, c** contour plots of the concentration modulus for pressure modulus and transportiveness (**b**) of filtration efficiency (**d**). The red-shaped regions refer to operation variables, for which the algebraic water flux equation is not valid. The arrows depict two hypothetical optimization scenarios.

Specifically, Fig. 5a is a map of equation (4), Fig. 5d is a map of equation (7), while Figure 5b, c are alternative representations of Fig. 5d, a, respectively. Several conclusions may be drawn about the strong or weak dependency of the variables on each other. For example, at a fixed value of P, the filtration efficiency can only be increased by increasing the mass transfer coefficient in the feed channel, hence higher K. On the other hand, at a fixed value of K, the filtration efficiency can partly be also increased by reducing P, that is, by working with a smaller driving force and a smaller overall productivity. To exemplify this discussion, a hypothetical optimization strategy may be assumed, in which an initial process with 80% filtration efficiency should be modified to reach a value of efficiency equal to 85%. If the process is characterized by $P = 6$, $K = 5.9$ (see starting point for the two arrows in Fig. 5a), the ECP can be reduced by moving into different directions. The red vertical arrow relates to the case where the feed pressure is held constant and K is increased, i.e., the cross-flow velocity. The blue horizontal arrow indicates the case whereby ECP is reduced by lowering the feed pressure at constant cross-flow velocity. Therefore, Fig. 5a suggests that the effect of K is more significant in influencing J than that of P. A strategy for optimizing a process in terms of filtration efficiency would thus favor adjusting the cross-flow velocity rather than the pressure. Similar to Fig. 1a, the orange region indicates ranges in P and K, for which the water flux equation is invalid.

Figure 5b–d indicate how J and the CP modulus change in the same optimization process. The initial process with 80% efficiency has a CP_{mod} of 2.2. When reducing the feed pressure at constant cross-flow (blue leftward arrow), the CP_{mod} drops to 1.1 as a

filtration efficiency of 85% is reached. In the case of increasing cross-flow at constant feed pressure, the CP_{mod} is instead reduced from 2.2 to 1.9. This observation implies that reducing the CP_{mod} can be very efficiently done by lowering the feed pressure, while increasing the cross-flow only has a limited effect. Note that the two outcomes in Fig. 5a, d are not in contradiction, but they actually suggest something less than trivial and related to the definitions of filtration efficiency and CP_{mod}. CP_{mod} indicates how much concentration exists at the membrane-feed interface, but it does not necessarily indicate how much water flux is lost with respect to ideality. On the other hand, J does not indicate what the concentration is at the membrane-feed interface, but rather how much the water flux will be reduced because of it.

Figure 5 may therefore be used to help design a filtration process. If the goal is maintaining a high filtration efficiency, thus allowing the correct exploitation of a certain driving force and membrane transport properties, the combinations of P and K can be determined from the maps for a certain target value of J. Based on the membrane properties and on the needed system productivity, one can then calculate the required values of the absolute design variables, p_f and k_d. Or alternatively, if the goal is to help choosing an appropriate membrane, the required value of A, that is, the most appropriate membrane for a certain application, can be estimated to achieve a certain fixed productivity or filtration efficiency, known or hypothesized as the operating conditions of a system.

In summary, the availability of a robust standard protocol for membrane characterization and a simple way to estimate the transport parameters from experimental data would incentivize

the adoption of common practices in the membrane field, with positive implications for membrane development and for the progress of science through clear and shared gathering, curation, and interpretation of data. Furthermore, an equation that allows for the straightforward estimation of the water flux across the active layer of dense membranes, without the need for numerical methods, would allow for the streamlined exploration of the productivity of a system under a wide range of operating conditions. It would also promote an understanding of the functioning of different membranes characterized by diverse transport parameters and comparison between membranes and materials. The equations proposed in this study include dimensionless parameters with physical meaning, all based on bulk values, and they are conceived so that their terms are strongly correlated to the efficiency of the process. Indeed, the highlight of the equation terms on system efficiency and the possibility to easily estimate the magnitude of concentration polarization allows for a better understanding of the performance of a system and of a membrane, beyond the sole assessment of productivity.

DATA AVAILABILITY

The data generated during the current study are found in the Supplementary Information.

REFERENCES

1. Tiraferri, A. et al. A method for the simultaneous determination of transport and structural parameters of forward osmosis membranes. *J. Memb. Sci.* **444**, 523–538 (2013).
2. Aschmoneit, F. J. & Hélix-Nielsen, C. Chapter 3—application of computational fluid dynamics technique in reverse osmosis/nanofiltration processes. *In:* Basile, A. & Ghasemzadeh, K. (eds.) Current trends and future developments on (Bio-) membranes, 63–79 (Elsevier, 2022).
3. Heiranian, M., DuChanois, R. M., Ritt, C. L., Violet, C. & Elimelech, M. Molecular simulations to elucidate transport phenomena in polymeric membranes. *Environ. Sci. Technol.* **56**, 3313–3323 (2022).
4. Aschmoneit, F. J. & Hélix-Nielsen, C. Omsd-an open membrane system design tool. *Sep. Purif. Technol.* **233**, 115975 (2020).
5. Biesheuvel, P., Dykstra, J., Porada, S. & Elimelech, M. New parametrization method for salt permeability of reverse osmosis desalination membranes. *J. Membr. Sci. Lett.* **2**, 100010 (2022).
6. Du, Y., Wang, Z., Cooper, N. J., Gilron, J. & Elimelech, M. Module-scale analysis of low-salt-rejection reverse osmosis: design guidelines and system performance. *Water Res.* **209**, 117936 (2022).
7. Oren, Y. S., Freger, V. & Nir, O. New compact expressions for concentration-polarization of trace-ions in pressure-driven membrane processes. *J. Membr. Sci. Lett.* **1**, 100003 (2021).
8. Freger, V. & Ramon, G. Z. Polyamide desalination membranes: formation, structure, and properties. *Prog. Polym. Sci.* **122**, 101451 (2021).
9. Asadollahi, M., Bastani, D. & Musavi, S. A. Enhancement of surface properties and performance of reverse osmosis membranes after surface modification: a review. *Desalination* **420**, 330–383 (2017).
10. Kingsbury, R., Wang, J. & Coronell, O. Comparison of water and salt transport properties of ion exchange, reverse osmosis, and nanofiltration membranes for desalination and energy applications. *J. Membr. Sci.* **604**, 117998 (2020).
11. Wijmans, J. & Baker, R. The solution-diffusion model: a review. *J. Membr. Sci.* **107**, 1–21 (1995).
12. Wang, L. et al. Salt and water transport in reverse osmosis membranes: beyond the solution-diffusion model. *Environ. Sci. Technol.* **55**, 16665–16675 (2021).
13. Wang, L. et al. Significance of co-ion partitioning in salt transport through polyamide reverse osmosis membranes. *Environ. Sci. Technol.* **57**, 3930–3939 (2023).
14. Biesheuvel, P., Rutten, S., Ryzhkov, I., Porada, S. & Elimelech, M. Theory for salt transport in charged reverse osmosis membranes: Nnovel analytical equations for desalination performance and experimental validation. *Desalination* **557**, 116580 (2023).
15. Kingsbury, R. S., Zhu, S., Flotron, S. & Coronell, O. Microstructure determines water and salt permeation in commercial ion-exchange membranes. *ACS Appl. Mater. Interfaces* **10**, 39745–39756 (2018).
16. Van Wagner, E. M., Sagle, A. C., Sharma, M. M. & Freeman, B. D. Effect of crossflow testing conditions, including feed ph and continuous feed filtration, on commercial reverse osmosis membrane performance. *J. Membr. Sci.* **345**, 97–109 (2009).
17. Hailemariam, R. H. et al. Reverse osmosis membrane fabrication and modification technologies and future trends: a review. *Adv. Colloid Interface Sci.* **76**, 102100 (2020).
18. Chen, J. C., Li, Q. & Elimelech, M. In situ monitoring techniques for concentration polarization and fouling phenomena in membrane filtration. *Adv. Colloid Interface Sci.* **107**, 83–108 (2004).
19. Mariñas, B. J. & Urama, R. I. Modeling concentration-polarization in reverse osmosis spiral-wound elements. *J. Environ. Eng.* **122**, 292–298 (1996).
20. Aschmoneit, F. J. & Hélix-Nielsen, C. Submerged-helical module design for pressure retarded osmosis: a conceptual study using computational fluid dynamics. *J. Membr. Sci.* **620**, 118704 (2021).
21. Baker, R. W. Membrane technology and applications (John Wiley & Sons, 2012).
22. Ritt, C. L. et al. The open membrane database: synthesis-structure-performance relationships of reverse osmosis membranes. *J. Membr. Sci.* **641**, 119927 (2022).
23. Srivathsan, G., Sparrow, E. M. & Gorman, J. M. Reverse osmosis issues relating to pressure drop, mass transfer, turbulence, and unsteadiness. *Desalination* **341**, 83–86 (2014).
24. Sutzkover, I., Hasson, D. & Semiat, R. Simple technique for measuring the concentration polarization level in a reverse osmosis system. *Desalination* **131**, 117–127 (2000).
25. Öner, G., Kabay, N., Güler, E., Kitiş, M. & Yüksel, M. A comparative study for the removal of boron and silica from geothermal water by cross-flow flat sheet reverse osmosis method. *Desalination* **283**, 10–15 (2011).
26. Wang, J. et al. A critical review of transport through osmotic membranes. *J. Membr. Sci.* **454**, 516–537 (2014).
27. Davenport, D. M. et al. Thin film composite membrane compaction in high-pressure reverse osmosis. *J. Membr. Sci.* **610**, 118268 (2020).
28. Kim, S. & Hoek, E. M. Modeling concentration polarization in reverse osmosis processes. *Desalination* **186**, 111–128 (2005).
29. Park, M., Park, J., Lee, E., Khim, J. & Cho, J. Application of nanofiltration pre-treatment to remove divalent ions for economical seawater reverse osmosis desalination. *Desalin. Water Treat.* **57**, 20661–20670 (2016).
30. Schäfer, A.I. & Fane, A.G. Nanofiltration: principles, applications, and new materials (John Wiley & Sons, 2021).
31. Hyung, H. & Kim, J.-H. A mechanistic study on boron rejection by sea water reverse osmosis membranes. *J. Membr. Sci.* **286**, 269–278 (2006).

AUTHOR CONTRIBUTIONS

A.T.: conceptualizing protocol, data analysis, writing of the manuscript. M.Ma.: generating experimental data, and writing the manuscript. M.Mo.: generating experimental data, and writing of the manuscript. M.G.: data analysis, writing of the manuscript. F.J.A.: conceptualizing & derivation of equations, writing of the manuscript

COMPETING INTERESTS

The authors declare no competing interests.

ADDITIONAL INFORMATION

Supplementary information The online version contains supplementary material available at https://doi.org/10.1038/s41545-023-00270-w.

Correspondence and requests for materials should be addressed to Fynn Jerome Aschmoneit.

Reprints and permission information is available at http://www.nature.com/reprints